Available online at www.sciencedirect.com

SciVerse ScienceDirect

Ceramics International 39 (2013) 7053–7061

CERAMICS INTERNATIONAL

www.elsevier.com/locate/ceramint

Electrochemical behaviour and sulfur tolerance of $V_xMo_{(1-x)}O_y$ as solid oxide fuel cell anode

Berceste Beyribey[a,*], Bora Timurkutluk[b,c], Tuğrul Y. Ertuğrul[b], Çiğdem Timurkutluk[b,c], Mahmut D. Mat[b]

[a]*Chemical Engineering Department, Yıldız Technical University, 34210 İstanbul, Turkey*
[b]*HYTEM, Mechanical Engineering Department, Nigde University 51245 Nigde, Turkey*
[c]*Vestel Defense Industry, Universiteler Mah, Titanyum Block 17/B Teknokent ODTU, 06800 Ankara, Turkey*

Received 8 December 2012; received in revised form 16 January 2013; accepted 15 February 2013
Available online 27 February 2013

Abstract

Vanadium molybdenum oxide system ($V_xMo_{(1-x)}O_y$ for $x \leq 0.13$) is synthesized through reducing acidified vanadate and molybdate solution at 60 °C by passing hydrogen sulfide gas through the solution. The electrochemical performance of the mixed oxide is tested at various operation temperatures as an anode material for intermediate temperature solid oxide fuel cell (IT-SOFC) under pure and 50 ppm H_2S-containing hydrogen fuel. The highest cell performance of 0.18 W cm^{-2} peak power is reached at an operation temperature of 750 °C for dry H_2. It is found that the addition of 50 ppm H_2S to the anode gas causes a 22% decrease in the cell peak power. The loss in the cell performance is attributed to both gas conversion and diffusion. Short-term regeneration tests indicate that 1 h-exposure to sulfur-free gas is insufficient for the reactivation of the cell performance.

Keywords: Solid oxide fuel cells; Hydrogen sulfide; Sulfur poisoning; Mixed ionic electronic conductor; Vanadium molybdenum oxide

1. Introduction

Intermediate temperature solid oxide fuel cells (IT-SOFCs) are promising energy conversion and generating systems due to their comparative advantages such as high efficiency, low emission, system compactness and flexibility of fuel selection. Unfortunately, anodes in IT-SOFCs are easily poisoned by the impurities in the gas streams, such as sulfur commonly present in natural gas [1,2]. Hydrogen sulfide (H_2S) is the most common impurity in these fuels [2] and recognized as a problem in operating IT-SOFCs with the conventional anodes such as Ni/Y_2O_3–ZrO_2 (Ni/YSZ), which is poisoned by H_2S rapidly and loss its activity for the electrochemical oxidation of hydrogen [3]. Therefore, the major technical challenge in IT-SOFCs for H_2S-containing fuels is to develop alternative anode materials that are both chemically and electrochemically stable, and catalytically active in H_2S-rich environments [3,4].

Various Ni-free materials have been tested for SOFCS as alternative sulfur-tolerant anodes, such as $BaTiO_3$ [3], $La_{0.4}Sr_{0.6}TiO_{3\pm\delta}$–$Y_{0.2}Ce_{0.8}O_{2-\delta}$ (LST–YDC) [5], $La_{0.75}Sr_{0.25}Cr_{0.5}Mn_{0.5}O_{3\pm\delta}$ (LSCM55) [1], $Ce_{0.9}Sr_{0.1}Cr_{0.5}Fe_{0.5}O_{3\pm\delta}$ (CSCrF) [6], $Ce_{0.9}Sr_{0.1}VO_x$ (CSV) [7] and $Co_{0.5}Fe_{0.5}$+$Sm_{0.2}Ce_{0.8}O_{1.9}$ (SDC) [8]. However, the most of these materials were found to be deactivated in H_2S-containing fuels due to the contents of various S species on the surface. Eventually, none of them provides all criteria that are required for a successful and effective anode with low polarization resistance and acceptable long-term stability [4].

Molybdenum dioxide (MoO_2) has been investigated for the partial oxidation of sulfur containing gasoline [9] and Jet-A fuel surrogate [10] and reported as an alternative high performance anode material for SOFCs due to its low cost, high catalytic activity, sulfur tolerance and metal-like electron conductivity [10]. Besides the molybdenum oxide,

*Corresponding author. Tel.: +90 212 383 4772; fax: +90 212 383 4725.
E-mail address: berceste@yildiz.edu.tr (B. Beyribey).

0272-8842/$ - see front matter © 2013 Elsevier Ltd and Techna Group S.r.l. All rights reserved.
http://dx.doi.org/10.1016/j.ceramint.2013.02.045

vanadium molybdenum oxide (V–Mo–O) system has also been studied on the partial oxidation of benzene [11,12], acrolein [13], crotonaldehyde [11]. These catalytically active V–Mo–O systems with high electronic and reduced ionic conductivity for low vanadium content lead us to investigate $V_xMo_{(1-x)}O_y$ mixed oxide and its sulfur-tolerance in IT-SOFCs as an alternative anode material. This paper presents the first results of electrochemical behavior and sulfur tolerance of $V_xMo_{(1-x)}O_y$ mixed oxide.

2. Experimental

2.1. Preparation of anode powder

$V_{0.13}Mo_{0.87}O_{2.935}$ mixed oxide powder was prepared as previously reported [14]. Hydrochloric acid (37%, Sigma–Aldrich) was added into the mix solution of ammonium heptamolybdate tetrahydrate ($(NH_4)_6Mo_7O_{24}\cdot 4\,H_2O$) (Merck) and ammonium monovanadate (NH_4VO_3) (Merck) to adjust pH to the desired value of ≤ 1. Hydrogen sulfide (H_2S) gas was bubbled through the solution heated to 60 °C during four hours. The produced $V_{0.13}Mo_{0.87}O_{2.935}$ were centrifuged and washed with distilled water and acetone and dried in air at 50 °C overnight.

2.2. Characterization of anode powder

Characterization of $V_{0.13}Mo_{0.87}O_{2.935}$ powder was described previously [14]. Thermogravimetry (TG), derivative thermogravimetry (DTG) and differential thermal analysis (DTA) were carried out using Perkin Elmer TG/DTA-6300 instrument. Thermal analysis experiment was performed in air (50 ml min^{-1}) with a heating rate of 5 °C min^{-1}. The measurement was done in the temperature range of room temperature to 1100 °C due to decomposition temperature of $V_{0.13}Mo_{0.87}O_{2.935}$ powder could not be defined with the thermal analysis up to 700 °C [14].

2.3. Electrolyte fabrication

ScSZ ($(ZrO_2)_{0.90}(Sc_2O_3)_{0.10}$) electrolyte was produced by tape casting. Commercial ScSZ powder (Nextech Materials) was mixed with an organic dispersant and solvent. After ball milling around 24 h, certain amount of plasticizer and binder were added. The mixture was ball milled again for another 24 h. Then the slurry was tape cast with a blade gap of 170 μm. Six tapes of ScSz electrolyte were stacked together and laminated isostatically under 40 MPa pressure for 10 min. The laminates were then cut into square (79 mm × 79 mm) using a laser cutter. The sintering of the electrolyte was performed at two stages. In the first stage, the electrolyte was heated to 1000 °C and held for 2 h. In the second stage, the electrolyte was sintered at 1400 °C for 4 h. The thickness of the electrolyte was measured as 150 μm after sintering whereas the outer dimensions were reduced to 60 mm × 60 mm.

2.4. Cell preparation and testing

LSCF ($(La_{0.60}Sr_{0.40})(Co_{0.20}Fe_{0.80})O_{3-\delta}$) (Nextech Materials) powder was used as the cathode material. LSCF powders were initially mixed with ethyl cellulose and terpineol at proper ratios (50 wt% solid loading) to prepare a cathode screen printing paste. After ball milling about 12 h, the cathode paste is screen printed on the electrolyte. The sintering of the cathode was achieved at 1050 °C for 2 h. The anode screen printing paste was prepared similarly and screen printed on the other side of the electrolyte symmetric to the cathode. After sintering the anode layer at 650 °C for 2.5 h, the cell was ready for testing. The active area of the cell was 16 cm^2 (4 cm × 4 cm).

The single cell was placed between two stainless steel interconnectors with nickel foam and stainless steel mesh which were respectively used as anode and cathode current collectors. The details of the short stack configuration can be found elsewhere [15–17]. All experiments were conducted in the temperature range of 650–750 °C. After the temperature was stable, various flow rates of hydrogen between 0.5–2.0 L min^{-1} were introduced to anode side of the single cell while ambient air was used as oxidant at the cathode side. The measurements were performed under dry hydrogen ($pH_2O < 0.001$ bar) and dry hydrogen containing 50 ppm hydrogen sulfide. Performance curves were obtained using a fuel cell test station (Arbin Instruments FCTS, TX, USA) which has a temperature controlled furnace with a push rod pressing capability to improve the contact between the cell and interconnectors. Electrochemical impedance spectra (EIS) were recorded under fuel cell test environment using a Parstat 2273 frequency response analyzer. Impedance measurements were carried out over the frequency range of 100 kHz to 0.01 Hz under open circuit voltage (OCV). Data analysis was done using the software *ZSimpWin 3.21*, supplied by Princeton Applied Research. Scanning Electron Microscopy (SEM), on the other hand, was through Carl Zeiss Evo 40.

3. Results and discussion

In order to investigate the thermal stability of metal oxide anode powder, thermogravimetric (TG) analysis and differential thermal analysis (DTA) were conducted. Fig. 1 illustrates the TG and DTA curves of $V_{0.13}Mo_{0.87}O_{2.935}$ mixed oxide. The TG curve in air displays two mass loss steps, which are attributed to the eliminating of adsorbed sulfur (between 30–380 °C) and the sublimation of MoO_3 formed by segregation of $V_{0.13}Mo_{0.87}O_{2.935}$ (between 750–795 °C). The mass loss values are 10 and 15 wt%, respectively. As seen in Fig. 1, DTA profile of the compound represents a large exothermic effect upon heating from room temperature to 750 °C. The reaction of adsorbed sulfur with oxygen and segregation of $V_{0.13}Mo_{0.87}O_{2.935}$ might be responsible of that exothermic effect. The

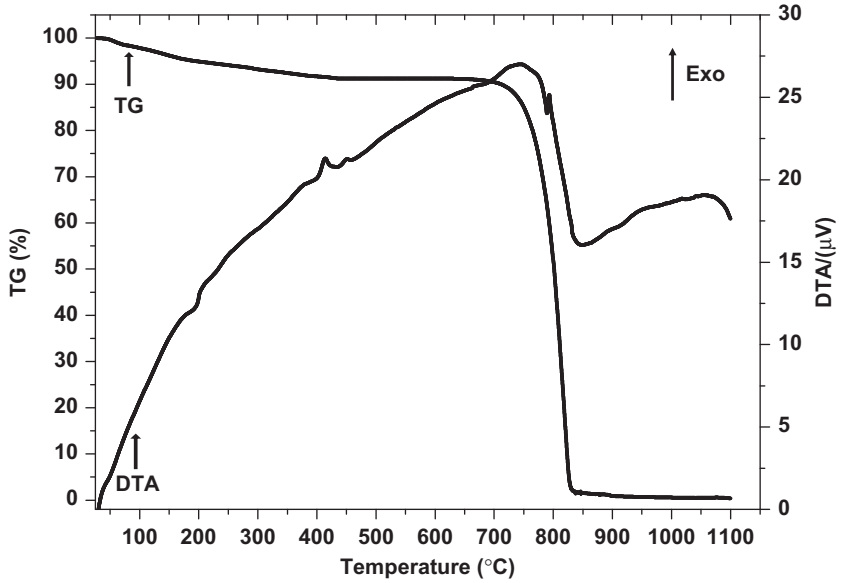

Fig. 1. Thermal analysis (TG and DTA) of the synthesized $V_{0.13}Mo_{0.87}O_{2.935}$ powder.

segregation of $V_{0.13}Mo_{0.87}O_{2.935}$ (above 600 °C) is given with the following reaction [18,19]:

$$V_{0.13}Mo_{0.87}O_{2.935} \rightarrow V_2MoO_8\text{-type phase} + MoO_3 \qquad (R1)$$

At higher temperatures, sublimation of MoO_3, which has a sublimation temperature of 795 °C [20], occurs and the mass loss reaches at 100 wt% by the temperature of 830 °C.

Fig. 2 shows the cell voltage and power density as a function of the current density at operation temperatures of 650, 700 and 750 °C for various dry hydrogen flow rates. It is seen that the cell performance tends to increase with increasing the hydrogen flow rate at all temperatures as expected. However, the effect of the hydrogen flow rate on the cell performance is highly significant at 650 °C operation temperature (Fig. 2(a)), comparing with that at higher operation temperatures can be seen at 700 and 750 °C operation temperatures (Fig. 2(b) and (c)). It seems concentration polarization is extremely effective limiting the cell performance at 650 °C operation temperature. Concentration polarization mainly dominates at low voltage regions (≤ 0.4 V) and as seen in Fig. 2(a), it surprisingly limits the cell performance at about 0.8 V in 0.5 L $min^{-1}H_2$ flow. By increasing the hydrogen flow rate, the cell performance enhances due to the decrease in the ohmic polarization while the concentration polarization still limits the cell performance at high voltages.

The single cell exhibited almost 1 W (~ 0.06 W cm^{-2}) maximum power output at 650 °C operation temperature when the hydrogen flow rate was set to the maximum (2 L min^{-1}). Similar behavior can be seen at 700 and 750 °C operation temperatures (Fig. 2(b) (c)). The highest cell performance was obtained at maximum hydrogen flow rate at both operation temperatures. The cell provides 1.76 W (~ 0.11 W cm^{-2}) and 2.88 W (0.18 W cm^{-2}) peak power at 700 °C and 750 °C, respectively. Moreover, concentration polarization finally dominates to limit the cell performance at low voltage region (~ 0.4 V) at 750 °C operation temperature. Furthermore, at all operation temperatures considered, the open circuit potential was around 1.17 V which was very close to the theoretical one indicating that the electrolyte is fully dense.

Fig. 3 shows the cell voltage and power density as a function of the current density at an operation temperature of 750 °C in dry H_2 and 50 ppm H_2S-containing dry H_2 with a flow rate of 2 L min^{-1}. The cell was first stabilized in pure hydrogen gas until a steady open circuit potential was observed. Then the current–voltage (*I–V*) and the current-power (*I–P*) curves were recorded under both dry H_2 and 50 ppm H_2S-containing dry H_2 to figure out the effect of H_2S on the cell performance. The results show that 50 ppm H_2S contamination causes a 22% decrease in the peak power density from 0.18 W cm^{-2} to 0.14 W cm^{-2} at 750 °C. Pillai et al. [21] tested a solid oxide fuel cell with Ni-YSZ anode supported on $Sr_{0.8}La_{0.2}TiO_3$ in H_2 containing 100 ppm H_2S and observed a 20% decrease in the peak power density at 800 °C. In a similar study, Kurokawa et al. [22] found ca. a 10% decrease in the power density at 800 °C, testing a SOFC with a Y-doped $SrTiO_3$ anode in 10 ppm H_2S-containing H_2. These results are comparable with the observation on the cell performance under H_2S-containing H_2 in this study.

After switching to sulfur-free gas (pure H_2) for 1 h, no reactivation of the cell was obtained. This means that the presence of 50 ppm H_2S in H_2 fuel degrades the performance of $V_xMo_{(1-x)}O_y$ anode at 750 °C and the degradation cannot be recovered by a short-term exposure to sulfur-free fuel gas. Zhang et al. [23] reported that even 5 ppm H_2S-containing H_2 fuel causes an unrecoverable degradation for Ni/YSZ anode, after treated under pure

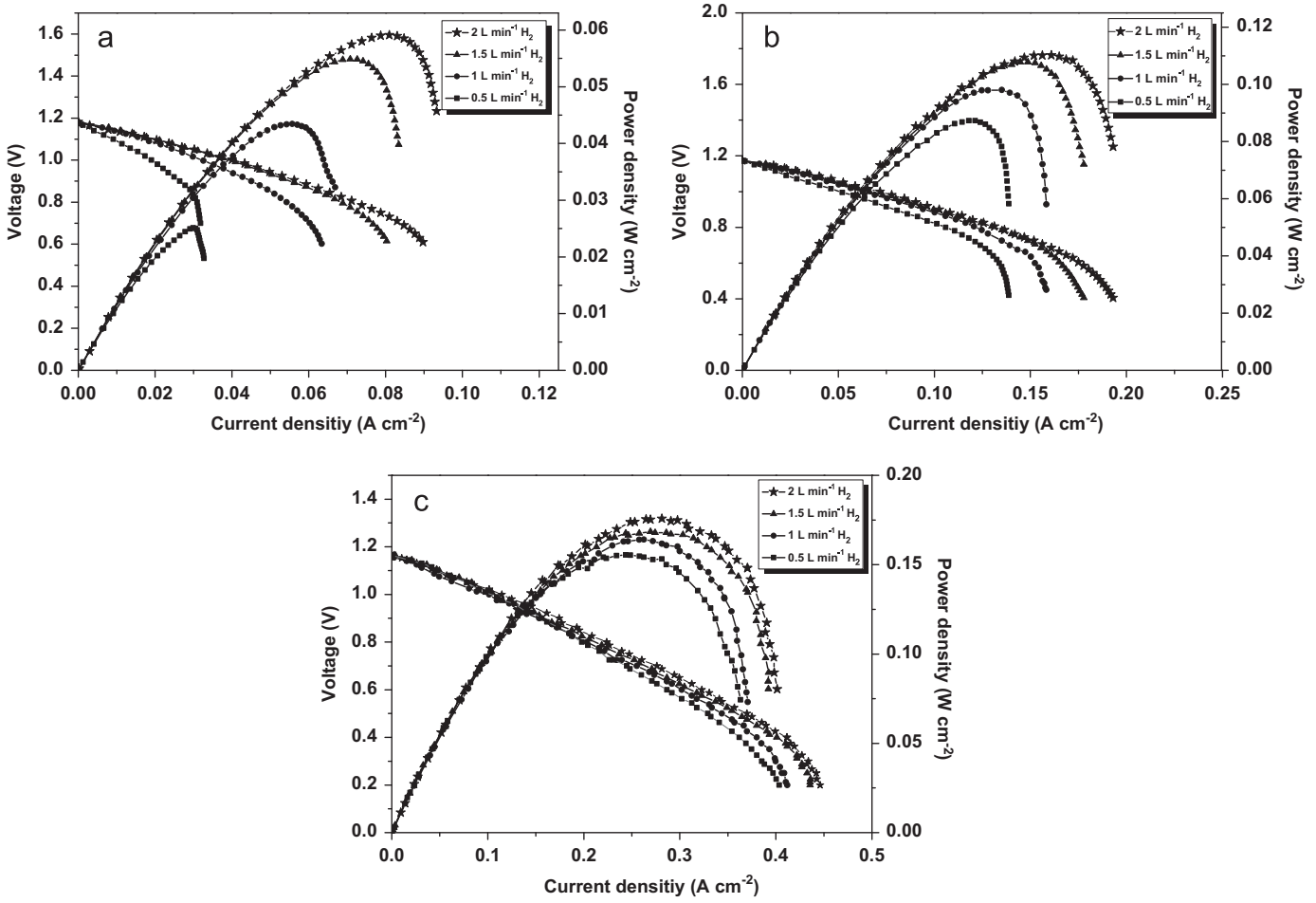

Fig. 2. The voltage and power density output versus the current density under various flow rates of dry H_2; (a) $T=650$ °C, (b) $T=700$ °C and (c) $T=750$ °C.

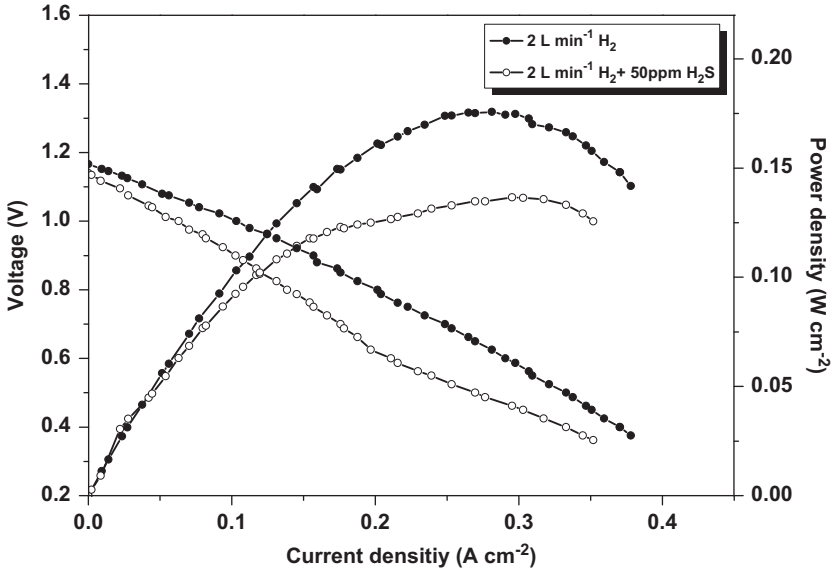

Fig. 3. The voltage and power density output versus the current density under flowing dry H_2 and 50 ppm H_2S-containing dry H_2. $T=750$ °C.

H_2 in a period of 2 h. On the other hand, Rasmussen et al. [24] found that for Ni/YSZ anodes which were subjected to 2 ppm H_2S-containing H_2 fuel, the recovery takes ~250 h, while Lohsoontorn et al. [25] showed 25 h-recovering time is necessary for Ni/GDC anodes after exposed to 1 ppm H_2S-containing H_2.

All EIS data represented in this paper were fitted to equivalent circuit model consisting of serially coupled $(RQ)^{\gamma}$ elements. The spectra were treated with as few $(RQ)^{\gamma}$ elements as possible. The general model is shown in Fig. 4. Similar models were used in the literature for comparable systems [16,26,27].

Fig. 5 denotes the measured resistances as function of the operation temperature in dry H_2 and it is seen that total resistivity of the single cell decreases with increasing temperature as expected. The model used to fit the impedance data is also shown in Fig. 5. The series resistance, R_s, arises mainly from the ionic conductivity of the electrolyte if the specific electronic conductivity of the electrode material is much higher than the specific ionic conductivity of the electrolyte [28]. The electrode response at higher frequencies is referred to as Arc 1, and its resistance and capacitance is denoted R_1 and C_1. Arc 1 probably relates ion transfer impedance at between the electrolyte and the electrode [28]. The low frequency response is referred to as Arc 2 which can be related to either gas diffusion or gas conversion [26], and its resistance and capacitance is denoted R_2 and C_2. The fitted parameters from impedance measurements of the cell with $V_xMo_{(1-x)}O_y$ anode are given in Table 1. Arc 2 is perfectly fitted with an n-value of unity indicates a process behaving like an ideal capacitor in parallel with a resistor at 650 and 700 °C. However it became depressed at 750 °C. Arc 2 has a rather large capacitance (C_2) of about 8–12 F cm^{-2} at 650 and 700 °C, while it suddenly decreased to 0.55 F cm^{-2} at 750 °C. This amount of decrease in capacitance may be attributed to the completion of the segregation of the anode material at about 750 °C (Fig. 1 and R1). Arc 1 is also found to be depressed at all temperatures. Capacitances are determined using the expression for all depressed arcs [29,30]:

$$C_{\omega} = R^{(1-n)/n} Q^{1/n} \quad (1)$$

Q is the constant phase element (CPE) and n is the frequency power observed from the fitting of the spectra. R_s values are found as 108 ± 1.52, 88 ± 1.24 and 78 ± 0.77 mΩ cm^2 at 650, 700 and 750 °C, respectively (Table 1). This indicates that R_s derived from the ohmic resistance is dependent on the temperature and decreases with the increasing temperature. As seen in Fig. 5, the high frequency response (Arc 1) with the summit frequency in

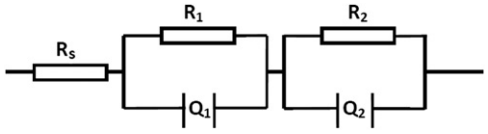

Fig. 4. Equivalent circuit model used fit the impedance spectra.

Table 1
Fitted parameters from the impedance measurements of the cell with $V_xMo_{(1-x)}O_y$ anode in pure H_2 and 50 ppm H_2S-containing H_2 at various temperatures.

	Pure H_2			50 ppm H_2S-containing H_2
	650 °C	700 °C	750 °C	750 °C
R_s (mΩ cm^2)	108 ± 2	88 ± 1	78 ± 0.8	77 ± 2
R_1 (mΩ cm^2)	286 ± 8	111 ± 3	20 ± 2	45 ± 9
C_1 (F cm^{-2})	0.038	0.039	0.052	0.028
n_1	0.67	0.71	0.83	0.77
R_2 (mΩ cm^2)	76 ± 8	83 ± 4	92 ± 5	329 ± 16
C_2 (F cm^{-2})	12.24	8.39	0.55	0.50
n_2	1	1	0.8	0.72

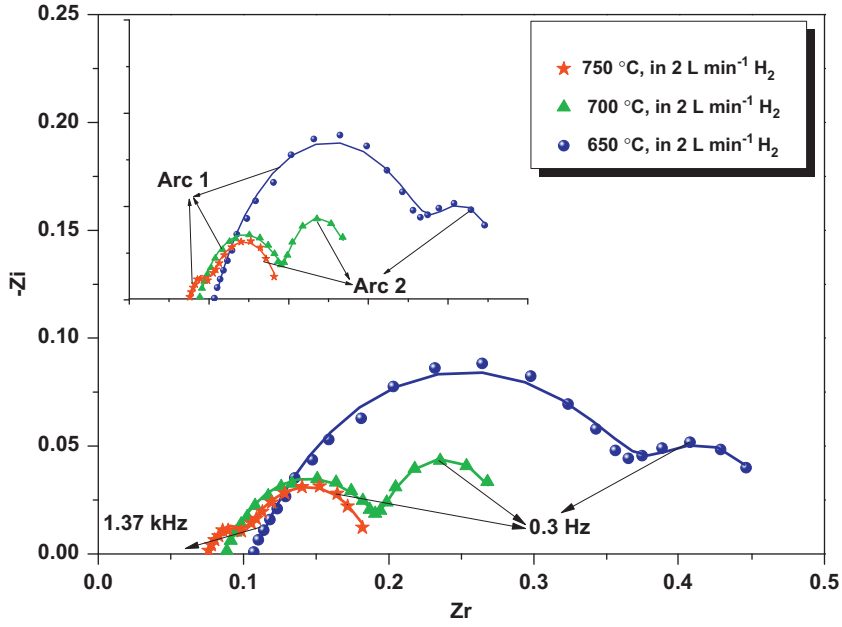

Fig. 5. Impedance spectra of the cell in dry H_2 at 650, 700 and 750 °C; symbols and lines respectively shows the measured values and the fittings by the model.

the range of 20–80 Hz can be assigned to diffusion (10 Hz-1 kHz) [31,32]. R_1 is found as $285.6 \pm 8.1\ m\Omega\ cm^2$ at 650 °C, $111.3 \pm 3.2\ m\Omega\ cm^2$ at 700 °C and $20 \pm 1.9\ m\Omega\ cm^2$ at 750 °C (Table 1). A low frequency response (Arc 2), with the summit frequency in the range of 0.3–1 Hz is not a thermally activated process and it means this process is not a part of the electrode reaction kinetics but reflects a concentration polarization [26] such as gas conversion at the anode (0.1–10 Hz) [33]. The value of R_2 is about 80–90 $m\Omega\ cm^2$ and relatively independent on the operation temperature. The decrease in the total resistance is found to be related mainly to R_1.

Fig. 6 represents the comparison of the impedance spectra at 750 °C in dry H_2 and 50 ppm H_2S-containing dry H_2, and the model used to fit the impedance data. $|Z|$ is plotted against the logarithmic frequency to demonstrate the difference in the cell before and after sulfur poisoning at 750 °C. The impedance spectra are different in frequency ranges below 4.52 Hz. This frequency range was reported to be related to diffusion and/or gas conversion at the anode (summit frequency below 10 Hz) [33,34]. As shown in Fig. 6, the sizes of the Arc 1 and Arc 2 respectively related to the gas conversion on the $V_xMo_{(1-x)}O_y$ anode and diffusion of the reactant from/to interface increase with the presence of H_2S in H_2. The significant increase of the Arc 2 indicates the substantial loss of the activity of the $V_xMo_{(1-x)}O_y$ anode for the H_2 oxidation reaction after H_2S-containing H_2 fuel due to the strong chemisorption of H_2S on the anode active sites. This result is compatible with previously reported results for the loss of the activity of Ni/YSZ anodes for H_2S-containing fuel [24].

Fig. 7 shows the SEM images of the anode surface before and after the test. According to the Fig. 7(a), the anode surface has a structure including needle and platelet crystals. It has been reported that $V_{0.13}Mo_{0.87}O_{2.935}$ crystals have a global needle or stick shape and vanadium content in $V_xMo_{1-x}O_y$ systems affects the dimensions of

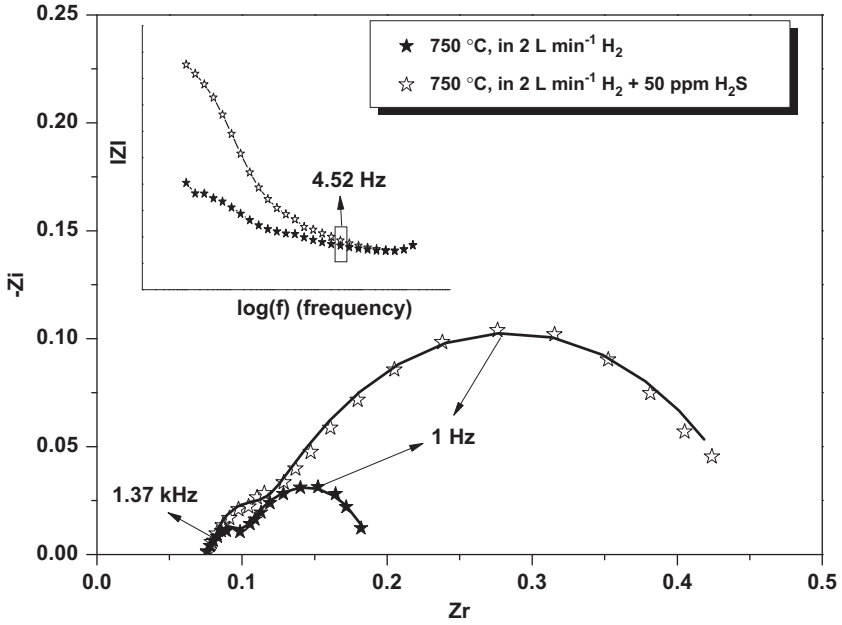

Fig. 6. The comparison of the impedance spectra of the cell in dry H_2 and 50 ppm H_2S-containing dry H_2 at 750 °C; symbols and lines respectively shows the measured values and fittings by the model.

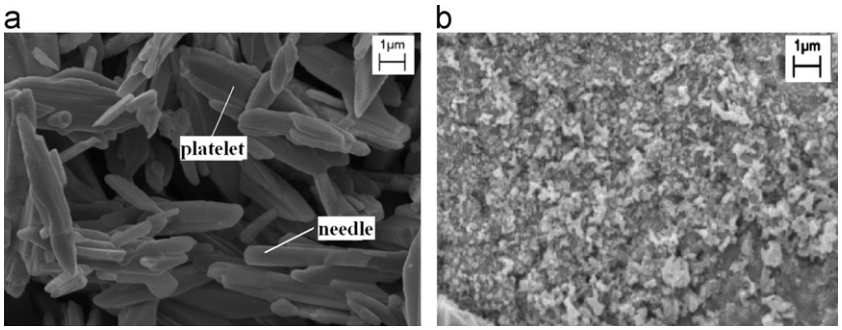

Fig. 7. SEM images of the anode surface; (a) pre-test and (b) post-test.

the needles [18,19]. Platelet crystals are formed above 600 °C by segregation between the vanadium and molybdenum takes place [19]. Sintering of the anode layer at 650 °C leads the formation of platelet crystals. During segregation, the vanadium goes away with some neighboring molybdenum and oxygen atoms, and the platelets of MoO_3 grow on the $V_{0.13}Mo_{0.87}O_{2.935}$ needles and/or sticks. The amount of vanadium decreases in the double layer and this mechanism lasts until all vanadium leaves the particle and MoO_3 is formed (Eq. (1)).

Fig. 7(b) shows the anode surface of the cell after than 4 h-testing in H_2 and 50 ppm H_2S-containing H_2. It can be clearly seen that the surface morphology of the cell tested with H_2 and H_2S-containing H_2 is significantly different from that of the fresh cell, indicating that H_2S decreased the performance of the system. MoO_2 and MoS_2 are formed by reducing of Mo(VI) species to Mo(IV) ones under H_2 (Eq. (2)) and H_2S-containing H_2 (Eq. (3)) atmospheres [9,35]:

$$MoO_3 + H_2 \leftrightarrow MoO_2 + H_2O \quad (2)$$

$$MoO_3 + 2H_2S + H_2 \leftrightarrow MoS_2 + 3H_2O \quad (3)$$

The anode surface of the tested cell presumably includes MoO_3, MoO_2 and MoS_2 particles. However, a decrease in the cell performance by forming of MoS_2 is not expected due to its high electronic conduction. MoS_2 has already tested as SOFC anode materials in H_2S-containing fuels [4,36,37] and was reported a good candidate as an anode material for H_2S-powered SOFC [4]. Therefore, instead of MoO_3, MoO_2 and MoS_2 formation, chemisorption of H_2S on the active sites of the anode surface can be related to the decrease in the cell performance. In addition to that, sulfur poisoning of the nickel foam used as the current collector on the anode side presumably contributes to the increase in the resistance of the cell. The surface of the nickel foam exposed to H_2S-containing fuel is poisoned by forming of Ni_xS and this leads to severe cracking, loss of mechanical strength and the significant increase in the electrical resistance [38].

Fig. 8 shows the effect of operation time on OCV of the cell at 750 °C operation temperature. The OCV values of the single cell in pure and 50 ppm H_2S-containing H_2 are compared in the figure. It is seen that the OCV value in pure H_2 is close to theoretical value and it is independent on the operation time. However, the OCV value decreases quickly after hydrogen sulfide is introduced into the fuel as expected for a short-term sulfur poisoning process [39].

4. Conclusion

The electrochemical behavior and sulfur tolerance of $V_xMo_{(1-x)}O_y$ mixed oxide were investigated as an anode material for solid oxide fuel cell. Performance measurements showed that the highest cell performance with a peak power of 2.88 W was observed at an operation temperature of 750 °C in dry H_2. It was found that 50 ppm H_2S contamination in dry H_2 caused a 22% decrease in the peak power and the deactivation process was found to be irreversible for a short-term exposure to sulfur-free gas. However, the reactivation of the cell may be achieved through a long-term hydrogen treatment which causes a reaction of hydrogen with adsorbed sulfur to form the volatile compound of H_2S.

Electrochemical impedance measurements resulted in two responses at high and low frequencies, respectively.

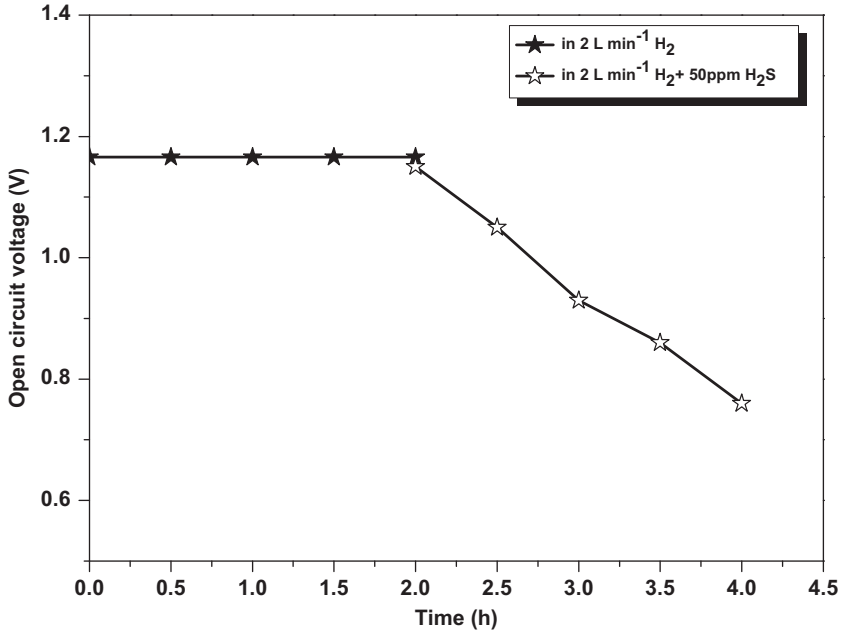

Fig. 8. The open circuit voltage (OCV) versus time in flowing pure and 50 ppm H_2S-containing H_2. T=750 °C.

The high frequency response was considered as a thermally activated process thus can be assigned to diffusion. The low frequency response, on the other hand, was relatively independent on temperature and attributed to the gas conversion on the anode surface. Furthermore, 50 ppm-H_2S contamination in dry H_2 negatively affected the electrode polarization resistance due to the chemical adsorption of the anode active sites and OCV value of the cell decreased linearly as expected for a typical short-term sulfur poisoning process [39].

Acknowledgment

This work was financially supported by Scientific Research Foundation of Yıldız Technical University and HYTEM Laboratory of Mechanical Engineering Department at Niğde University.

References

[1] T. Wenyi, Z. Qin, Y. Han, Z. Xiufang, L. Hongyi, Deactivation of anode catalyst $La_{0.75}Sr_{0.25}Cr_{0.5}Mn_{0.5}O_{3\pm\delta}$ in SOFC with fuel containing hydrogen sulfur: the role of lattice oxygen, International Journal of Hydrogen Energy 37 (2012) 7398–7404.

[2] L.L. Zheng, X. Wang, L. Zhang, J.-Y. Wang, S.P. Jiang, Effect of Pd-impregnation on performance, sulfur poisoning and tolerance of Ni/GDC anode of solid oxide fuel cells, International Journal of Hydrogen Energy 37 (2012) 10299–10310.

[3] J.-H. Li, X.-Z. Fu, J.-L. Luo, K.T. Chuang, A.R. Sanger, Application of $BaTiO_3$ as anode materials for H_2S containing CH_4 fueled solid oxide fuel cells, Journal of Power Sources 213 (2012) 69–77.

[4] V. Vorontsov, W. An, J.L. Luo, A.R. Sanger, K.T. Chuang, Performance and stability of composite nickel and molybdenum sulfide based anodes for SOFC utilizing H_2S, Journal of Power Sources 179 (2008) 9–16.

[5] M. Roushanafshar, J.-L. Luo, A.L. Vincent, K.T. Chuang, A.R. Sanger, Effect of hydrogen sulfide inclusion in syngas feed on the electrocatalytic activity of LST-YDC composite anodes for high temperature SOFC applications, International Journal of Hydrogen Energy 37 (2012) 7762–7770.

[6] X. Zhu, H. Yan, Q. Zhong, X. Zhao, W. Tan, $Ce_{0.9}Sr_{0.1}Cr_{0.5}Fe_{0.5}O_{3\pm\delta}$ as the anode materials for solid oxide fuel cells running on H_2 and H_2S, Journal of Alloys and Compounds 509 (2011) 8360–8364.

[7] N. Danilovic, J.-L. Luo, K.T. Chuang, A.R. Sanger, $Ce_{0.9}Sr_{0.1}VO_x$ (x=3,4) as anode materials for H_2S containing CH_4 fueled solid oxide fuel cells, Journal of Power Sources 192 (2009) 247–257.

[8] Z.G. Lu, J.H. Zhu, Z.H. Bi, X.C. Lu, A Co–Fe alloy as alternative anode for solid oxide fuel cell, Journal of Power Sources 180 (2008) 172–175.

[9] O.G.M. Flores, S. Ha, Activity and stability studies of MoO_2 catalyst for the partial oxidation of gasoline, Applied Catalysis A: General 352 (2009) 124–132.

[10] O.G.M. Flores, T. Turba, C. Ellefson, L. Scudiero, J. Breit, M.G. Norton, S. Ha, Sulfur poisoning of molybdenum dioxide during the partial oxidation of a Jet-A fuel surrogate, Applied Catalysis B: Environmental 105 (2011) 61–68.

[11] V. Lochař, H. Drobná, FTIR study of the interaction of crotonaldehyde and maleic anhydride with V_2O_5 and MoO_3, Applied Catalysis A: General 269 (1-2) (2004) 27–31.

[12] Y.H. Taufiq-Yap, K.C. Waug, A study of the nature of the oxidant in V_2O_5–MoO_3/Al_2O_3 Catalyst, Chemical Engineering Science 56 (2001) 5787–5792.

[13] J. Tichỳ, Oxidation of acrolein to acrylic acid over vanadium–molybdenum oxide catalysts, Applied Catalysis A: General 157 (1997) 363–385.

[14] B. Beyribey, A new way of synthesis of hexagonal $V_{0.13}Mo_{0.87}O_{2.935}$ and an investigation on its structural, thermal and anodic properties, Research on Chemical Intermediates (2012)http://dx.doi.org/10.1007/s11164-012-0676-9.

[15] B. Timurkutluk, S. Celik, C. Timurkutluk, M.D. Mat, Y. Kaplan, Novel electrolytes for solid oxide fuel cells with improved mechanical properties, International Journal of Hydrogen Energy 37 (2012) 13499–13509.

[16] B. Timurkutluk, S. Celik, C. Timurkutluk, M.D. Mat, Y. Kaplan, Novel structured electrolytes for solid oxide fuel cells, Journal of Power Sources 213 (2012) 47–54.

[17] B. Timurkutluk, S. Celik, S. Toros, C. Timurkutluk, M.D. Mat, Y. Kaplan, Effects of electrolyte pattern on mechanical and electrochemical properties of solid oxide fuel cells, Ceramics International 38 (2012) 5651–5659.

[18] O. Mougin, J.L. Dubois, F. Mathieu, A. Rousset, Metastable hexagonal vanadium molybdate study, Journal of Solid State Chemistry 152 (2) (2000) 353–360.

[19] L. Dupont, D. Larcher, M. Touboul, The phase transitions between $H_{0.13}V_{0.13}Mo_{0.87}O_3\cdot 0.26H_2O$ and MoO_3: an X-ray, thermal analysis, and TEM study, Journal of Solid State Chemistry 143 (1999) 41–51.

[20] R.H. Perry, D.W. Green, Perry's Chemical Engineer's Handbook, 7th Ed., Mc Graw Hill, New York, 1997.

[21] M.R. Pillai, I. Kim, D.M. Bierschenk, S.A. Barnett, Fuel-flexible operation of a solid oxide fuel cell with $Sr_{0.8}La_{0.2}TiO_3$ support, Journal of Power Sources 185 (2008) 1086–1093.

[22] H. Kurokawa, L. Yang, C.P. Jacobson, L.C. De Jonghe, S.J. Visco, Y-doped $SrTiO_3$ based sulfur tolerant anode for solid oxide fuel cells, Journal of Power Sources 164 (2007) 510–518.

[23] L. Zhang, S.P. Jiang, H.Q. He, X. Chen, J. Ma, X.C. Song, A comparative study of H_2S poisoning on electrode behavior of Ni/YSZ and Ni/GDC anodes of solid oxide fuel cells, International Journal of Hydrogen Energy 35 (2010) 12359–12368.

[24] J.F.B. Rasmussen, A. Hagen, The effect of H_2S on the performance of Ni–YSZ anodes in solid oxide fuel cells, Journal of Power Sources 191 (2009) 534–541.

[25] P. Lohsoontorn, D.J.L. Brett, N.P. Brandon, The effect of fuel composition and temperature on the interaction on H_2S with nickel–ceria anodes for solid oxide fuel cells, Journal of Power Sources 183 (2008) 232–239.

[26] P. Hjalmarsson, M. Søgaard, M. Mogensen, Electrochemical behavior of $(La_{1-x}Sr_x)_sCo_{1-y}Ni_yO_{3-\delta}$ as porous SOFC cathodes, Solid State Ionics 180 (2009) 1395–1405.

[27] P. Hjalmarsson, M. Søgaard, M. Mogensen, Electrochemical performance and degradation of $(La_{0.6}Sr_{0.4})_{0.99}CoO_{3-\delta}$ as porous SOFC-cathode, Solid State Ionics 179 (2008) 1422–1426.

[28] P. Blennow, K.K. Hansen, L.R. Wallenberg, M. Mogensen, Effects of Sr/Ti-ratio in $SrTiO_3$-based SOFC anodes investigated by the use of cone-shaped electrodes, Electrochimica Acta 52 (2006) 1651–1661.

[29] F.W. Poulsen, N. Bonanos, S. Linderoth, M. Mogensen, B. Zachau-Christiansen, High Temperature Electrochemistry: Ceramics and Metals, in: Proceedings of the 17th Risø International Symposium on Materials Science, Risø National Laboratory, Roskilde, Denmark, 1996.

[30] B. Beyribey, J. Hallinder, Structural, thermal and electrical studies of a novel rubidium phosphite tellurate compound, Ceramics International 38 (2012) 5095–5102.

[31] S.D. Ebbesen, M. Mogensen, Electrolysis of carbon dioxide in solid oxide electrolysis Cells, Journal of Power Sources 193 (2009) 349–358.

[32] S. Primdahl, M. Mogensen, Gas diffusion impedance in characterization of solid oxide fuel cell anodes, Journal of The Electrochemical Society 146 (1999) 2827–2833.

[33] S. Primdahl, M. Mogensen, Gas conversion impedance: a test geometry effect in characterization of solid oxide fuel cell anodes, Journal of The Electrochemical Society 145 (1998) 2431–2438.

[34] R. Barfod, A. Hagen, S. Ramousse, P.V. Hendriksen, M. Mogensen, Break down of losses in thin electrolyte SOFCs, Fuel Cells 6 (2006) 141–145.
[35] P. Afanasiev, Synthetic approaches to the molybdenum sulfide materials, Comptes Rendus Chimie 11 (2008) 159–182.
[36] M. Liu, G. Wei, J. Luo, A.R. Sanger, K.T. Chuang, Use of metal sulfides as anode catalysts in H_2S–air SOFCs, Journal of The Electrochemical Society 150 (2003) A1025–A1029.
[37] M. Liu, H_2S-powered solid oxide fuel cells, PhD Thesis, University of Alberta, 2004.
[38] Q.X. Low, W. Huang, X.Z. Fu, J. Melnik, J.L. Luo, K.T. Chuang, A.R. Sagner, Copper coated nickel foam as current collector for H_2S-containing syngas solid oxide fuel cells, Applied Surface Science 258 (2011) 1014–1020.
[39] K. Haga, S. Adachi, Y. Shiratori, K. Itoh, K. Sasaki, Poisoning of SOFC anodes by various fuel impurities, Solid State Ionics 179 (2008) 1427–1431.